ACS APPLIED MATERIALS & INTERFACES

Article

Novel porous polyurea network showing aggregation induced white light emission, applications as biosensor and scaffold for drug delivery

Subhajit Bhunia, Nabanita Chatterjee, Subhadip Das, Krishna Das Saha, and Asim Bhaumik

ACS Appl. Mater. Interfaces, **Just Accepted Manuscript** • DOI: 10.1021/am5066859 • Publication Date (Web): 02 Dec 2014

ACS Applied Materials & Interfaces is published by the American Chemical Society.
1155 Sixteenth Street N.W., Washington, DC 20036

Novel Porous Polyurea Network Showing Aggregation Induced White Light Emission, Applications as Biosensor and Scaffold for Drug Delivery

Subhajit Bhunia,[a] Nabanita Chatterjee,[b] Subhadip Das,[b] Krishna Das Saha[b] and Asim Bhaumik[*,a]

[a]*Department of Material Science, Institution Association for the Cultivation of Science, Jadavpur, Kolkata-700032, India, *Corresponding author. E-mail: msab@iacs.res.in*

[b]*Cancer Biology and Inflammatory Disorder Division, CSIR-Indian Institute of Chemical Biology, Jadavpur, Kolkata-700032, India*

Abstract

We have designed a novel nanoporous polyurea network material POP-PU, which showed aggregation induced white light emission in the presence of suitable polar solvents. This nanomaterial has been explored as pseudo-white light emitter where the polymeric luminogen moiety can interact with the suitable polar solvent leading to charge transfer. Thus, solvent assisted rotational freezing of non rigid polymeric nanoparticles gives the radiative emission and the whole solution emitted white light with color temperature of 8533 K. This nanoporous material also holds the pockets (DDA array) for specific bio-molecular interaction. Among three pyrimidine based nucleotide bases only cytosine can amplify the PL emission intensity of POP-PU but other two bases can't, suggesting its future potential as biosensor. Further, this urea functionalized porous organic nanomaterial can be utilized as an efficient drug-delivery vehicle for liver cancer diagnostics and therapy based on the specific biomolecular interaction at its surface.

Keywords: Biosensor; drug delivery; organic white light emitter; polyurea network; porous organic polymer.

Introduction

Responsive polymeric materials, which can form supramolecular nanostructures in the presence of external stimuli are attracting increasing interests over the years due to their diverse range of demanding applications, such as drug delivery, diagnostics, 'smart' optical systems, biosensors and so on.[1] Among the polymers, porous organic polymers (POPs),[2-9] which combine the surface porosity of the material and reactive organic functional groups of the framework are rapidly developing class of material due to the tunability of the pore aperture and the diversity of the functional groups that could present in the framework building blocks. POPs are typically prepared through polymerization/ condensation,[10-12] cyclization[13] or metal mediated coupling/addition or hydrothermal reactions.[14-16] Although the organic functional groups present in these POPs are mostly utilized for gas storage and catalytic applications,[17,18] their specific interaction with solvent molecules leading to solvatochromic behaviour, gelation, aggregation induced emission,[19] biosensing and related biomedical applications are not explored so far. However, there is hardly any report on porous organic polymer, which could show aggregation induced white light emission in the presence of a solvent.

Genosensors or nucleic acid probe-based biosensors, which utilize the interaction of the nucleic acid with the ligand binding sites are very important for genome mapping and gene sequence analysis.[20] If phenyl and pyrimidine nucleus are interconnected through the urea (-NHCONH-) functionality, resulting poly-urea network bearing the DDA (Donor-Donor-Acceptor) array can interact via Hydrogen-bond to enhanced binding affinity to a complementary AAD array and may cause photoluminescence signal amplification for the nucleotide bases.[21,22] In this context it is pertinent to mention that porous organic polymers have not been explored in theranostics for anti-cancer drugs. Such nano-technological advancement is highly demanding in pharmaceutical and drug industry.[23] Mesoporous silica, metal oxides, metal organic frameworks (MOFs) and many organic polymeric micelles are employed for controlled drug

delivery in recent times.[24,25] From the inorganic platform gold, platinum nanoparticles are most effective drug delivery carrier due to their inertness. However, their non-biodegradability is often a serious issue when accumulated in human body. From the viewpoint of cost and biodegradability organic polymeric nanoparticles are superior than inorganic metal and ceramic nanoparticles. Although, organic liposomal drug delivery is a clinically established method but it has serious drawbacks like low encapsulation efficiency, fast release of drugs, poor storage stability and lack of tunable triggers for drug release.[26] Organic polymeric nanoparticles such as polylactide–polyglycolide copolymers, polyacrylates and polycaprolactones are other smart nano-systems known for drug delivery due to the change in its physicochemical properties in response to environmental signals and their biodegradability. However, these systems are devoid of any bio-sensing or white light emission property.

Herein, we first report the synthesis of a pyrimidine containing urea functionalized porous organic polymer material POP-PU through the organic sol-gel reaction of 2,4,6-triaminopyrimidine and 1,4-phenylene diisocyanate followed by agglomeration to obtain pyrimidyl urea network material,[27] which showed solvent dependent white light emission property. Addition of excess amount of non-solvent to the sol produced through the reaction between 2,4,6-triaminopyrimidine and 1,4-phenylene-diisocyanate yield organic nanomaterial POP-PU (Fig. 1). Here we have shown a new nanoporous organic biodegradable polyurea network obtained from simple one step synthetic process which can be used as an excellent carrier for drug delivery and simultaneously enhances the efficiency of the anticancer drug and liver cancer therapeutics. Due to the presence of DDA array in POP-PU it can interact strongly with cycloheximide, which could facilitate its potential as drug-delivery carrier. Further, the fluorescence property of POP-PU persuades a promising biomedical application, especially the intervention of theranostics approach in liver cancer prevention.[28,29] The ‘apoptotic trigger’ in cancer cells is considered as the keynote phenomenon of cancer therapy.[30,31] Considering all these unique

features we have explored the three-in-one application potentials of novel multifunctional material POP-PU as i) white light emitter, ii) genosensor for the nucleotide base cytosine and iii) a drug delivery vehicle for the liver cancer diagnostics and therapy using cycloheximide as a model drug.

Result and discussion:

FTIR absorption band at 1632 cm^{-1} for POP-PU could be attributed to the C=O stretching frequency, whereas 3299 and 1220 cm^{-1} bands are assigned due to the N-H and C-N stretching frequencies as shown in Fig 2a. Absence of peak corresponding to primary -NH_2 group in the FTIR spectrum of POP-PU suggested complete condensation between amine and isocyanate groups in this POP-PU network. Chemical environment of different carbon atoms of the constituent moieties of the POP-PU framework has been analyzed from the respective solid state ^{13}C CP MAS NMR spectrum as shown in Fig. 2b. POP-PU showed strong signals corresponding to the presence of phenyl (C_5, C_6 and C_7) and pyrimidine (C_1, C_2 and C_4) rings and these are interconnected through urea group (C_3). The N_2 adsorption/desorption isotherms at 77 K for POP-PU follows the type IV isotherm (Fig. 3) together with a noticeable desorption hysteresis loop corresponding to random mesopores. The Brunauer–Emmett–Teller (BET) surface area of the POP-PU is 142 m^2g^{-1}. Pore size distribution of POP-PU using the nonlocal density functional theory (NLDFT) and carbon slit pore model suggested trimodal porosity with peaks at 1.5, 2.8, and 4.5 nm (Fig 3, inset). From the nature of the adsorption isotherm mesoporosity in the POP-PU material is quite evident. X-ray diffraction pattern of POP-PU is shown in Fig S1 (ESI), where one broad peak at 2θ = 2.2 degree corresponding to a disordered mesophase is observed. Further sharp peaks at 2θ = 11.9, 20.6 and 21.6 degrees suggested semicrystalline nature of the polymeric network of POP-PU (inset of Fig. S1, ESI).

HRTEM images of POP-PU material obtained via non-solvent induced agglomeration have been shown in Fig. 4. From these images it is clear that POP-PU possesses hair like nanofibre morphology having hair length of *ca*.75-140 nm and width of *ca*. 5 nm. These nanofibres are uniformly distributed throughout the specimen grid. The internal void spaces between the nanoparticles could be the origin of wide range of porosity (supermicropores to mesopores) in POP-PU. It is pertinent to mention that nanoporous organic polymer with white light emission in the aggregate or solid state is rare because aggregation of polymer generally quenches light emission. Here this new polyurea network of POP-PU bearing pyrimidine and phenylene ring has been generated through the reaction of the amine and isocyanate groups. Large amount of acetone was added as non-solvent to prepare the organic sol and to agglomerate the particles to the nanoscopic range (75-140 nm). The material is virtually nonluminiscent in solid state but the dilute solution of POP-PU in DMF originates the white light emission property. The intrinsic photoluminescence of POP-PU in water under ultraviolet excitation (at 378 nm) showed strong emission at wavelengths between 390 nm and 520 nm. The most compulsive fact is that the nonfluorescent material transforms to bluish-white light emitter in DMF with the CIE coordinate (0.26, 0.38) and the colour temperature (8533 K). Corresponding photoluminescence spectrum has been shown in Fig. 5b. It showed three humps at 433, 484 and 532 nm and thus, suggesting the white colour is a three colour white. This type of radiative emission is attributed to the fact of DMF assisted freezing of single-bond rotational freedom of urea functionalized network (Fig. 5a). PL spectra in $CHCl_3$ and acetone showed very poor emission, whereas emission intensity has drastically amplified in DMSO, DMF and EtOH (Fig. 6a). Respective photographs are shown in Fig. 6b. The enthalpy of interaction of urea with DMF and similar solvent like DMAc is exceptionally large than other solvents.[32] So the conformationally flexible network is rigidified in DMF and DMAc to a greater extend. As the non radiative energy loss due to flexibility of bond rotation are restricted abruptly in DMF and DMAc. So

the intrinsic nonfluorescent nanofibre gains the white light emitting property in the solution phase. High concentration of the individual building blocks in POP-PU in the presence of DMF solvent resulted supramolecular polymeric assembly via charge-transfer (Fig S2, ESI).[33,34] Considerable increase in average particle size vis-à-vis that in water suggested aggregation of POP-PU in DMF. Thus, this porous polymer backbone may be rigidified by virtue of a series of Hydrogen bonds between urea moiety[35,36] and the solvent molecules (Fig. 5a) leading to restriction of the intramolecular rotation and the material behaves like a solid-state luminogen to cause aggregation-induced emission (AIE).[37] Restricted geometry of the donor and acceptor moieties of POP-PU in the presence of DMF solvent could induce physical constraint in the supramolecular polymeric backbone, which minimize the non-radiative energy losses of their excitons and maximize their probability of radiative transitions leading to white light emission. This property is prominent in DMF.[38-40] Thus, although the building blocks in solvents are nonemissive, the network polymers are highly luminescent in various solvents and such three colour white light emitters based on metal-free porous polymeric material is very demanding.

POP-PU as Biosensing of Cytosine:

Further, POP-PU have the functionality containing appropriate hydrogen bonding array (donor-donor-acceptor) in the framework and thus we have examined its possibility for recognizing cytosine (Fig. 7a), an important hydrogen bonding unit for DNA binding. The binding between cytosine and POP-PU had been studied by taking the photoluminescence spectra of same amount of POP-PU sample in different concentrations of aqueous solutions of cytosine. As seen from the figure that large enhancement of PL intensity is observed with increasing concentration of cytosine.[41,42] The experiment has also been carried out using other pyrimidine bases thymine and uracil. But for the last two cases significant decrease of PL intensity is observed (Fig. 7b-c). It is pertinent to mention that photoluminescence spectrum of only cytosine suggests that cytosine is totally non-fluorescent. Thus, the

enhancement of PL intensity is not due to fluorescence from cytosine. Biosensors based on mesoporous materials are very demanding today.[43] Thus, POP-PU can act as a solid-state biosensor for the selective sensing cytosine when it is present along with the three pyrimidine based nucleotide bases. Since, the functional architecture of the POP-PU material holds the pocket to interact with nucleotide bases, this material can be employed as nanocarrier for drug-delivery. The nucleotide bases interact with the material through complementary H-bonded interactions. So the drug molecules like, cytarabine, cycloheximide etc., which have the resemblance of structure with nucleotide bases can undergo complimentary H-bonding with the tris (urea)pyrimidine moiety of the host material (Fig. 8a). Based on such interaction we have explored the POP-PU material as a drug delivery vehicle using cycloheximide, a well-known protein synthesis inhibitor as a model drug in the following section.

POP-PU as Drug Delivery vehicle for Cycloheximide:

The presence of H-bond donor and acceptor sites in close vicinity in POP-PU have been explored for their capability of binding with many anticancer drugs (cytarabine), protein synthesis inhibitors (cycloheximide) and thus can be used as a nanocarrier.[44,45] We have shown the possible interaction between cycloheximide (model anticancer drug) and POP-PU material in Fig. 8b. To triggering the apoptotic efficacy, cycloheximide loaded POP-PU (POP-PU-CHX) (0-0.02 nM) was evaluated for its cytotoxic property in cancer cells (Fig. 9a). However, the POP-PU was not effective to elicit any significant cytotoxicity. The results of cell cytotoxicity assay indicated that there was no variation for the two different type cells like normal cells and cancerous cells with POP-PU only. POP-PU-CHX reduced the viability of $HepG_2$ cells with GI50 of 0.01256 ± 0.00344 considerably after 36 h in comparison with only cyclohexamide (Fig. 9b)

Mitochondrial integrity or the loss of membrane potential (Ψ_m) has been linked to the initiation and activation of the series of apoptotic cascade with synchronized release of cytochrome C. Fluorescence emission shift of the Ψm sensitive cationic JC-1 dye. Cells were treated with 0.02 nM of POP-PU-CHX and stained with JC-1, cells showed the potential depolarization of mitochondrial membrane. Detailed biological studies over POP-PU have been illustrated in ESI section S1 and Figures S3-S6.

Nanomedicine: Apoptosis inducing effect of cycloheximide loaded POP-PU:

For triggering the apoptotic efficacy, cycloheximide loaded POP-PU (POP-PU-CHX) (0-0.02 nM) was evaluated for its cytotoxic property in cancer cells (Fig. S3, ESI). However, the POP-PU was not effective to elicit any significant cytotoxicity. The results of cell cytotoxicity assay indicated that there was no variation for the two different type cells like normal cells and cancerous cells with POP-PU only (Fig. S3). To confirm the apoptosis induction effect against cancer cell afforded by the POP-PU-CHX, annexin-PI cytometry assay were conducted in $HepG_2$ cells. POP-PU-CHX rapidly reduced the viability of $HepG_2$ cells with GI50 of 2.34 ± 0.59 after 36 h in comparison with only cyclohexamide channelized in $HepG_2$ cells that geared up the release of annexin from cell membrane and afforded apoptosis as found in Fig. 10b. An intercellular instance phosphatidyl serine exposure was sequentially correlated with nuclei fragmentation stained with DAPI as evident from the Fig.10a. The reflection of apoptosis also was found in cell cycle arrest (Fig. 11) in the treatment of the cells with 0.02 nM of the POP-PU-CHX for 0 h, 12 h, 24 h and 36 h. This study confirms that the POP-PU-CHX induces apoptosis in $HepG_2$ cells at lower concentration than cycloheximide alone.

Cellular uptake study with Cycloheximide loaded on POP-PU:

Cellular uptake studies were performed to ascertain whether the internalization of POP-PU-CHX in $HepG_2$ cells. Florescence images (Figure 12a) revealed the localization of POP-PU-CHX within cytosolic region of cells at concentration 0.02 nM in 36 h, that simultaneously instantiated the fluorophore property and results cellular apoptosis. The accumulation of POP-PU-CHX (0.02 nM) was also evidenced and confirmed in $HepG_2$ cells in time-dependent through FACS analysis (Figure 12b). These results suggested that POP-PU-CHX may be explored as a novel lipids and DNA. The molecular approach of fluorophore in POP-PU-CHX having the cell detecting properties together with its therapeutic intervention is very challenging in the context of cancer research.

Effect of POP-PU-CHX in mitochondrial membrane potential with cytochrome C and caspases:

Photostable AIE luminogens have been employed for mitochondrial imaging and tracking. Mitochondrial integrity or the loss of membrane potential (Ψ_m) has been linked to the initiation and activation of the series of apoptotic cascade with synchronized release of cytochrome C.[46] We have investigated whether POP-PU-CHX would be able to generate oxidative stress by means of measuring ROS in spectrofluorimetric analysis. As shown in Figure S5 (ESI), we found POP-PU-CHX (0.02 nM) significantly induced a huge amount of ROS in $HepG_2$ cell at 36 h. Thus, galvanized process precedes the apoptotic sequential occurrence including loss of mitochondrial membrane potential (Ψ_m) and increase of cytosolic cytochrome C release that altered the pro and anti apoptotic proteins levels with simultaneous activation of the caspase series. To determine whether POP-PU-CHX induced apoptosis in $HepG_2$ cells involves mitochondrial disruption, we have examined the depolarization of mitochondrial membrane by measuring the fluorescence emission shift of the Ψ_m sensitive cationic JC-1 dye. Cells were treated with 0.02 nM of POP-PU-CHX and stained with JC-1, cells showed the potential depolarization of mitochondrial membrane (Figure 12c). Significantly increment of cytochrome C release in cytosolic portion (Figure S6A, ESI) was balanced with the reduced amount in

mitochondrial portion (Figure S6B, ESI) in $HepG_2$ cells as quantified by ELISA. Generation of excessive reactive oxygen species (ROS) is one of the potent causes to induce apoptosis leading to cell death through the damage of cellular proteins. Therefore, POP-PU-CHX elicited the activation of initiator caspase 9 and effectors of caspase 3 in HepG2 cells as shown in Figure S6C (ESI). These results indicate that POP-PU-CHX induces the cellular apoptosis via ROS mediated mitochondrial pathway.

Experimental Section

Powder X-ray diffraction (XRD) patterns of POP-PU samples were analyzed with a Bruker D8 Advance X-ray diffractometer using Ni–filtered Cu Kα (λ=0.15406 nm) radiation. N_2 adsorption desorption isotherms were recorded on Autosorb 1C (Quantachrome Instruments, USA) at 77 K. High resolution transmission electron microscopic (HRTEM) images of the porous polymers were obtained using a JEOL JEM 2010 transmission electron microscope operating at 200 kV voltage. UV-Vis spectrum of POP-PU was recorded in a Shimadzu UV-2401PC doubled beam spectrophotometer having an integrating sphere attachment for solid samples. Photoluminescence spectra of the POP-PU in were taken in a Horiba fluorolog 3. Carbon, hydrogen and nitrogen contents were determined by Perkin Elmer 2400 Series II CHN analyzer.

1. Materials:

2, 4, 6 triaminopyrimidine and 1,4 phenylene diisocyanate were procured from Sigma Aldrich and anhydrous DMF was obtained from Spectrochem, India. Other reagents are purchased from Merck, India.

Synthesis of POP-PU nanopowder:

The synthesis of POP-PU was carried out by the sol-gel microimulsion technique to obtain the nanoscopic organic material. 250 mg (2 mmol) 2, 4, 6 triaminopyrimidine and 480 mg (3 mmol) 1,4-phenylene diisocyanate was refluxed in 35 ml anhydrous DMF at 428 K under N_2 atmosphere for 2 days. The reaction mixture was cooled to room temperature which gives orange colored suspension. Then the polymeric nanoparticle was obtained by the agglomeration technique. 350 ml acetone (non-solvent) was poured into reaction mixture and stirred for 1h. The turmeric colour precipitate was collected through vacuum filtration and successively washed with acetone, ethanol, THF, methanol. The obtained powder material was dried at 353 K under vacuum to obtain POP-PU. The yield is 54% (400 mg) based on 2,4,6 triaminopyrimidine and 1,4 phenylene diisocyanate. Elemental analysis found by combustion: C, 51.9%; H, 5.40%; N, 24.53%. Calcd. Theoretical formula from an infinite POP-PU framework $[C_{25}H_{22}N_8O_3]_n$: C, 62.23%; H, 4.6%; N, 23.22%.

Genosensing application:

20 mg of POP-PU sample was sonicated in 20 ml deionised water for 1 h. Then that stock solution was added to 1 ml to each cuvette containing nucleotide bases of different concentration prepared in deionised water. The experiment had been carried out for three different pyrimidine nucleotide bases; thymine, uracil, cytosine. Each time the excitation wavelength was 378 nm.

In vitro cell imaging and cellular uptake studies:

Cell imaging studies was carried out using the $HepG_2$ cell line which was maintained proper cell culture condition. To study the cellular uptake of POP-PU-CHX, cells (1×10^4/well) were grown on 30 mm Petri dish well plates for 24 h at 37 °C and 5% CO_2 followed by incubation with POP-PU-CHX in cell culture medium for 36 h. After fixation, cells were acquired by confocal laser scanning (Revolution

XD Spinning Disk with an iXon 897 EMCCD camera; Andor, Belfast, UK) after 36 h incubation; cellular uptake study revealed that POP-PU-CHX was internalized by the cell membrane leading to cytosolic portion of cell. Cellular uptake experiments were conducted according to a literature method with some modifications. After exposure to 0.02 nM of POP-PU-CHX for 12, 24 and 36 h, the cells was taken and uptake study was performed by FACS analyzer (BD LSRFortessa). For the details of the experimental employed for the cell culture, MTT assay, fluorescence imaging, changes in the mitochondrial membrane potential, estimation of intracellular ROS. Caspase-3, caspase -9 and cytochrome c assay please see the electronic supporting information (ESI).

Conclusions

A new porous polyurea based nanomaterial has been synthesized through organic sol-gel reaction between 2,4,6 triaminopyrimidine and 1,4 phenylene diisocyanate followed by the non-solvent induced aggregation. The resulting porous polymer showed high BET surface area, mesoporosity and solvent induced white light emission. This novel material has been explored in three frontline areas of energy and biomedical research, i) pseudo-white light emitter due to solvent induced aggregation; ii) selective biosensing of cytosine and iii) high efficacy as a drug-delivery vehicle for therapy and diagnostics of cancer drug cycloheximide due to the presence of fluorophore moiety, nanoscale porosity and intrinsic binding sites, suggesting its future potential in energy and biomedical research.

Acknowledgment

SB wishes to thank CSIR, New Delhi for a Junior Research Fellowship. AB wishes to thank DST, New Delhi for DST-SERB project grant. Authors are thankful to Dr S.N. Bhattacharya and Mr. D. Sarkar for confocal microscopy. K.D.S. thanks Prof. S. Roy, the Director CSIR-IICB and CSIR for necessary supports.

Supporting Information:

Small angle PXRD, wide angle PXRD, dynamic light scattering study, biological study, characterization, data interpretation are provided in this section. This information is available free of charge via the Internet at http://pubs.acs.org/.

References

(1) Stuart, M. A. C.; Huck, W.T. S.; Genzer, J.; Müller, M.; Ober, C.; Stamm, M.; Sukhorukov, G. B.; Szleifer, I.; Tsukruk, V. V.; Urban, M.; Winnik, F.; Zauscher, S.; Luzinov, I.; Minko, S. Emerging Applications of Stimuli-Responsive Polymer Materials. *Nat. Mater*. **2010**, *9*, 101-113.

(2) Côté, A. P.; Benin, A. I.; Ockwig, N. W.; Keeffe, M. O'.; Matzger, A. J.; Yaghi, O. M. Porous, Crystalline, Covalent Organic Frameworks. *Science* **2005**, *310*, 1166-1170.

(3) Chandra, D.; Jena, B. K.; Raj, C. R.; Bhaumik, A. Functionalized Mesoporous Cross-Linked Polymer as Efficient Host for Loading Gold Nanoparticles and Its Electrocatalytic Behavior for Reduction of H_2O_2. *Chem. Mater.* **2007**, *19*, 6290-6296.

(4) Uribe-Romo, F. J.; Hunt, J. R.; Furukawa, H.; Klöck, C.; O'Keeffe, M.; Yaghi, O. M. A Crystalline Imine-Linked 3-D Porous Covalent Organic Framework. *J. Am. Chem. Soc.* **2009**, *131*, 4570-4571.

(5) Dawson, R.; Laybourn, A.; Clowes, R.; Khimyak, Y. Z.; Adams, D. J.; Cooper, A. I. Functionalized Conjugated Microporous Polymers. *Macromolecules* **2009**, *42*, 8809-8816.

(6) Rabbani, M. G.; El-Kaderi, H. M. Template-Free Synthesis of a Highly Porous Benzimidazole-Linked Polymer for CO_2 Capture and H_2 Storage. *Chem. Mater.* **2011**, *23*, 1650-1653.

(7) Modak, A.; Mondal, J.; Bhaumik, A. Porphyrin Based Porous Organic Polymers: Novel Synthetic Strategy and Exceptionally High CO_2 Adsorption Capacity. *Chem. Commun.* **2012**, *48*, 248-250.

(8) Thiel, K.; Zehbe, R.; Roeser, J.; Strauch, P.; Enthaler, S.; Thomas, A. A Polymer Analogous Reaction for the Formation of Imidazolium and NHC Based Porous Polymer Networks. *Polym. Chem.* **2013**, *4*, 1848-1856.

(9) Kang, N.; Park, J.H.; Ko, K.C.; Chun, J.; Kim, E.; Shin, H. W.; Lee, S. M.; Kim, H. J.; Ahn, T. K.; Lee, J. Y.; Son, S. U. Tandem Synthesis of Photoactive Benzodifuran Moieties in the Formation of

Microporous Organic Networks. *Angew. Chem. Int. Ed.* **2013**, *52*, 6228-6232.

(10) Bhunia, M. K.; Das, S. K.; Pachfule, P.; Banerjee, R.; Bhaumik, A. Nitrogen-Rich Porous Covalent Imine Network (CIN) Material as an Efficient Catalytic Support for C–C Coupling Reactions. *Dalton Trans.* **2012**, *41*, 1304-1311.

(11) Katsoulidis, A. P.; Kanatzidis, M. G. Mesoporous Hydrophobic Polymeric Organic Frameworks with Bound Surfactants. Selective Adsorption of C_2H_6 versus CH_4. *Chem. Mater.* **2012**, *24*, 471-479.

(12) Modak, A.; Pramanik, M.; Inagaki, S.; Bhaumik, A. A Triazine Functionalized Porous Organic Polymer: Excellent CO_2 Storage Material and Support for Designing Pd Nanocatalyst for C–C Cross-Coupling Reactions. *J. Mater. Chem. A* **2014**, *2*, 11642-11650.

(13) Islamoglu, T.; Rabbani, M. G.; El-Kaderi, H. M. Impact of Post-Synthesis Modification of Nanoporous Organic Frameworks on Small Gas Uptake and Selective CO_2 Capture. *J. Mater. Chem. A* **2013**, *1*, 10259-10266.

(14) Cheng, G.; Hasell, T.; Trewin, A.; Adams, D. J.; Cooper, A. I. Soluble Conjugated Microporous Polymers. *Angew. Chem. Int. Ed.* **2012**, *51*, 12727-12731.

(15) Lee, D.; Zhang, C. Y.; Wei, C.; Ashfeld, B. L.; Gao, H. F. Hierarchically Porous Materials *via* Assembly of Nitrogen-Rich Polymer Nanoparticles for Efficient and Selective CO_2 Capture. *J. Mater. Chem. A* **2013**, *1*, 14862-14867.

(16) Kubo, S.; White, R. J.; Tauer, K.; Titirici, M. M. Flexible Coral-like Carbon Nanoarchitectures via a Dual Block Copolymer–Latex Templating Approach. *Chem. Mater*. **2013**, *25*, 4781-4790.

(17) Moon, S. –Y.; Bae, J. –S.; Jeon, E.; Park, J. –W. Organic Sol–Gel Synthesis: Solution-Processable Microporous Organic Networks. *Angew. Chem. Int. Ed.* **2010**, *49*, 9504-9508.

(18) Suresh, V. M.; Bonakala, S.; Atreya, H. S.; Balasubramanian, S.; Maji, T. K. Amide

Functionalized Microporous Organic Polymer (Am-MOP) for Selective CO_2 Sorption and Catalysis. *ACS Appl. Mater. Interfaces* **2014**, *6*, 4630-4637.

(19) Liu, Y.; Tao, X.; Wang, F.; Dang, X.; Zou, D.; Ren, Y.; Jiang, M. Aggregation-Induced Emissions of Fluorenonearylamine Derivatives: A New Kind of Materials for Nondoped Red Organic Light-Emitting Diodes. *J. Phys. Chem. C* **2008,** *112,* 3975-3981.

(20) Beattie, K. L.; Beattie, W. G.; Meng, L.; Turner, S. L.; Coral-Vazquez, R.; Smith, D. D.; McIntyre, P. M.; Dao, D. D. Advances in Genosensor Research. *Clin. Chem*. **1995**, *41*, 700-706.

(21) Abbel, R.; Grenier, C.; Pouderoijen, M. J.; Stouwdam, J. W.; Leclére, P. E. L. G.; Sijbesma, R. P.; Meijer, E. W.; Schenning, A. P. H. J. White-Light Emitting Hydrogen-Bonded Supramolecular Copolymers Based on π-Conjugated Oligomers. *J. Am. Chem. Soc.* **2008**, *131*, 833-843.

(22) Lei, J.; Ju, H. Signal Amplification Using Functional Nanomaterials for Biosensing. *Chem. Soc. Rev.* **2012**, *41*, 2122-2134.

(23) Farokhzad, O. C.; Langer, R. Impact of Nanotechnology on Drug Delivery. *ACS Nano* **2009**, *3*, 16-20.

(24) Zhang, Q.; Liu, K.; Nguyen, T.; Ma, X.; Wang, X.; Xing, B.; Zhao, Y. Multifunctional Mesoporous Silica Nanoparticles for Cancer-Targeted and Controlled Drug Delivery. *Adv. Funct. Mater*. **2012**, *22*, 5144-5156.

(25) Sen, T.; Sheppard, S. J.; Mercer, T.; Eizadi-Sharifabad, M.; Elhissi, A. Simple One-pot Fabrication of Ultra-Stable Core-Shell Superparamagnetic Nanoparticles for Potential Application in Drug Delivery. *RSC Adv*. **2012**, *2*, 5221-5228.

(26) Bamrungsap, S.; Zhao, Z.; Chen, T.; Wang, L.; Li, C.; Fu, T.; Tan, W. Nanotechnology in Therapeutics. *Nanomedicine* **2012**, *7*, 1253-1271.

(27) Quinn, J. R.; Zimmerman, S. C. With Regard to the Hydrogen Bonding in Complexes of

Pyridylureas, Less is More. A Role for Shape Complementarity and CH···O Interactions?. *Org. Lett.* **2004**, *6*, 1649-1652.

(28) Yu, Y.; Tan, S.; Zhao, S.; Zhuang, X.; Song, Q.; Wang, Y.; Zhou, Q.; Zhang, Z. Antitumor Activity of Docetaxel-loaded Polymeric Nanoparticles Fabricated by Shirasu Porous Glass Membrane-Emulsification Technique. *Int. J. Nanomed.* **2013**, *8*, 2641-2652.

(29) Ma, D. L.; He, H. Z.; Leung, K. H.; Chan, D. S. H.; Leung, C. H. Bioactive Luminescent Transition-Metal Complexes for Biomedical Applications. *Angew. Chem. Int. Ed*. **2013**, *52*, 7666-7682.

(30) Lee, J. E.; Lee, N.; Kim, H.; Kim, J.; Choi, S. H.; Kim, J. H.; Kim, T.; Song, I. C.; Park, S. P.; Moon, W. K.; Hyeon, T. Uniform Mesoporous Dye-Doped Silica Nanoparticles Decorated with Multiple Magnetite Nanocrystals for Simultaneous Enhanced Magnetic Resonance Imaging, Fluorescence Imaging, and Drug Delivery. *J. Am. Chem. Soc*. **2010**, *132*, 552-557.

(31) Pramanik, M.; Chatterjee, N.; Das, S.; Saha K. D.; Bhaumik, A. Anthracene-Bisphosphonate Based Novel Fluorescent Organic Nanoparticles Explored as Apoptosis Inducers of Cancer Cells. *Chem. Commun*. **2013**, *49*, 9461-9463.

(32) Noodleman, L.; Norman, J.G. Jr., Osborne, J.H.; Aizman, A.; Case, D.A. Models for Ferredoxins: Electronic Structures of Iron-Sulfur Clusters with One, Two, and Four Iron Atoms. *J. Am. Chem. Soc.* **1985**, *107*, 3418-3426.

(33) Čejková, J.; Štěpánek, F. Compartmentalized and Internally Structured Particles for Drug Delivery-a Review. *Curr. Pharma. Des.* **2013**, *19*, 6298-6314.

(34) Leung, C. W. T.; Hong, Y. N.; Chen, S. J.; Zhao, E. G.; Lam, J. W. Y.; Tang, B. Z. A Photostable AIE Luminogen for Specific Mitochondrial Imaging and Tracking. *J. Am. Chem. Soc.* **2013**, *135*, 62-65.

(35) Chu, W.-J.; Chen, J.; Chen, C.-F.; Yang, Y.; Shuai, Z. Amidourea-Based Hydrogen-Bonded Heteroduplexes: Structure and Assembling Selectivity. *J. Org. Chem.* **2012**, *77*, 7815-7822.

(36) Aida, T.; Meijer, E. W.; Stupp, S. I. Functional Supramolecular Polymers. *Science* **2012**, *335*, 813-817.

(37) Hong, Y.; Lam, J. W. Y.; Tang, B. Z. Aggregation-Induced Emission. *Chem. Soc. Rev.* **2011**, *40*, 5361-5388.

(38) Xu , Y. H.; Chen, L.; Guo, Z. Q.; Nagai, A.; Jiang, D. L. Light-Emitting Conjugated Polymers with Microporous Network Architecture: Interweaving Scaffold Promotes Electronic Conjugation, Facilitates Exciton Migration, and Improves Luminescence. *J. Am. Chem. Soc.* **2011**, *133*, 17622-17625.

(39) Bairi, P.; Roy, B.; Chakraborty, P.; Nandi, A. K. Co-Assembled White-Light-Emitting Hydrogel of Melamine. *ACS Appl. Mater. Interfaces* **2013**, *5*, 5478-5485.

(40) Shustova, N. B.; Cozzolino, A. F.; Dinca, M. Conformational Locking by Design: Relating Strain Energy with Luminescence and Stability in Rigid Metal–Organic Frameworks. *J. Am. Chem. Soc*. **2012**, *134*, 19596-19599.

(41) Yang, M.; McGovem, M. E.; Thompson, M. Genosensor Technology and the Detention of Interfacial Nucleic Acid Chemistry. *Anal. Chim. Acta* **1997**, *346*, 259-275.

(42) Ho, A. H.; Dore, K.; Boissinot, M.; Bergeron, M. G.; Tanguay, R. M.; Boudreau, D.; Leclerc, M. Direct Molecular Detection of Nucleic Acids by Fluorescence Signal Amplification. *J. Am. Chem.* Soc. **2005**, *127*, 12673-12676.

(43) Mondal, K.; Ali, M. A.; Agrawal, V. V.; Malhotra, B. D.; Sharma, A. Highly Sensitive Biofunctionalized Mesoporous Electrospun TiO_2 Nanofiber Based Interface for Biosensing. *ACS Appl. Mater. Interfaces* **2014**, *6*, 2516-2527.

(44) Das, S. K.; Bhunia, M. K.; Chakraborty, D.; Khuda-Bukhsh, A. R.; Bhaumik, A. Hollow Spherical Mesoporous Phosphosilicate Nanoparticles as a Delivery Vehicle for an Antibiotic Drug. *Chem. Commun*. **2012**, *48*, 2891-2893.

(45) Fang, Y.; Zheng, G. F.; Yang, J. P.; Tang, H. S.; Zhang, Y. F.; Kong, B.; Lv, Y. Y.; Xu, C. J.; Asiri, A. M.; Zi, J.; Zhang, F.; Zhao, D. Y. Dual-Pore Mesoporous Carbon@Silica Composite Core–Shell Nanospheres for Multidrug Delivery. *Angew. Chem. Int. Ed*. **2014**, *53*, 5366-5370.

(46) Gomez-Crisostomo, N. P.; Lopez-Marure, R.; Zapata, E.; Zazueta, C.; Martinez-Abundis, E. Bax Induces Cytochrome c Release by Multiple Mechanisms in Mitochondria from MCF7 Cells. *J Bioenerg. Biomembr.* **2013**, *45*, 441-448.

Caption for Figures:

Figure 1 Reaction of 2,4,6 triaminopyrimidine and 1,4 phenylene diisocyanate under organic sol-gel conditions and agglomeration at the nanoscale to produce POP-PU.

Figure 2 a) FTIR spectra of 2,4,6 triaminopyrimidine, 1,4 phenylene diisocyanate, POP-PU b) ^{13}C solid state CP MAS NMR spectrum of POP-PU.

Figure 3 N_2 adsorption/desorption isotherms of POP-PU nanomaterial. Adsorption points are marked by filled and desorption points by empty circle and Pore size distribution employing NLDFT method (inset).

Figure 4 HRTEM images of POP-PU nanofibres at different magnifications.

Figure 5 a) Strong H-bonding interaction between POP-PU and DMF, b) PL spectrum of POP-PU+DMF and CIE coordinate (exitation at 378 nm).

Figure 6 a) PL spectra of POP-PU material in different solvent (excitation at 375 nm) b) photographic images of POP-PU in different solvents after photoexcitaton.

Figure 7 Photoluminescent spectra of a) cytosine-POP-PU (amplifying); b) thymine-POP-PU (quenching) and c) uracil-POP-PU under condition (quenching). 2 ml 0.04 wt% aqueous solution of POP-PU has been used for all the analyses. Excitation wavelength was 378 nm.

Figure 8 a) Interaction of cytosine with POP-PU having DDA array (left). b) Possible H-bonding interaction between POP-PU and protein biosynthesis inhibitor (cycloheximide, right).

Figure 9 (a) Cells were treated with POP-PU in the concentration range (0 – 0.02 nM) of CHX, POP-PU-CHX for 36 h. The significance result was found with POP-PU-CHX as compared to CHX. (b) Effect of POP-PU-CHX on Annexin V-FITC binding in HepG2 cells in different time including 0 h, 12 h, 24 h and 36 h and denotations like Q1, Q2, Q3 and Q4 are identified as necrotic cells, late apoptotic cells, live cells and apoptotic cells.

The data are represented as mean ± SEM from triplicate independent experiments.

Figure 10 a) Morphological changes were observed in HepG2 cells after 0.02 nM the treatment of POP-PU-CHX treatment for 36 h and seen under fluorescence microscopy after DAPI staining (Scale bar 10µm). b) Annexin V-FITC binding in HepG2 cells in different time including 0 h, 12 h, 24 h and 36 h. The data are represented as mean ± SEM (*P<0.05, **P<0.01) of triplicate independent experiments.

Figure 11 Cell cycle analysis up to 36 h with the concentration of 0.02 nM. The data are represented as mean ± SEM (*P<0.05, **P<0.01) of triplicate independent experiments.

Figure 12 a) Effect of POP-PU-CHX on HepG2 cells and cell imaging by POP-PU-CHX at concentration of 0.02 nM treatment using confocal laser microscopy with accurate laser. Scale bar 10µm. (b) Cellular uptake studies: % cellular uptake of POP-PU-CHX by HepG2 cells with increasing time (h) demonstrate as spectrofluorimetric analysis. c) Effect of POP-PU-CHX on $HepG_2$ cells on Membrane potential evaluated with JC-1 dye reactively by confocal image.

Figure 1

.

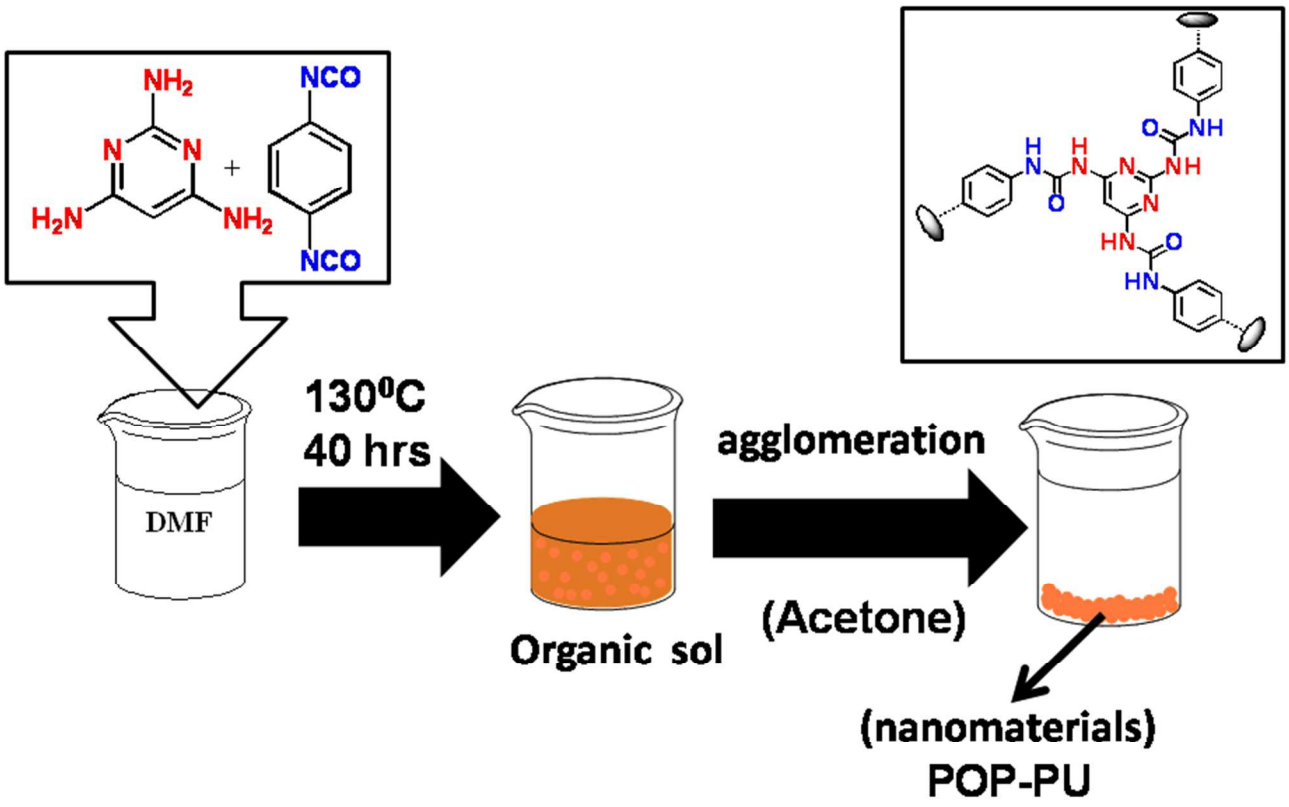
NH2
NCO
N
N
H2N
NH2
NCO
+
DMF
130⁰C
40 hrs
Organic sol
agglomeration
(Acetone)
(nanomaterials)
POP-PU
O
NH
H
N
N
O
N
NH
N
HN
O
HN

Figure 2

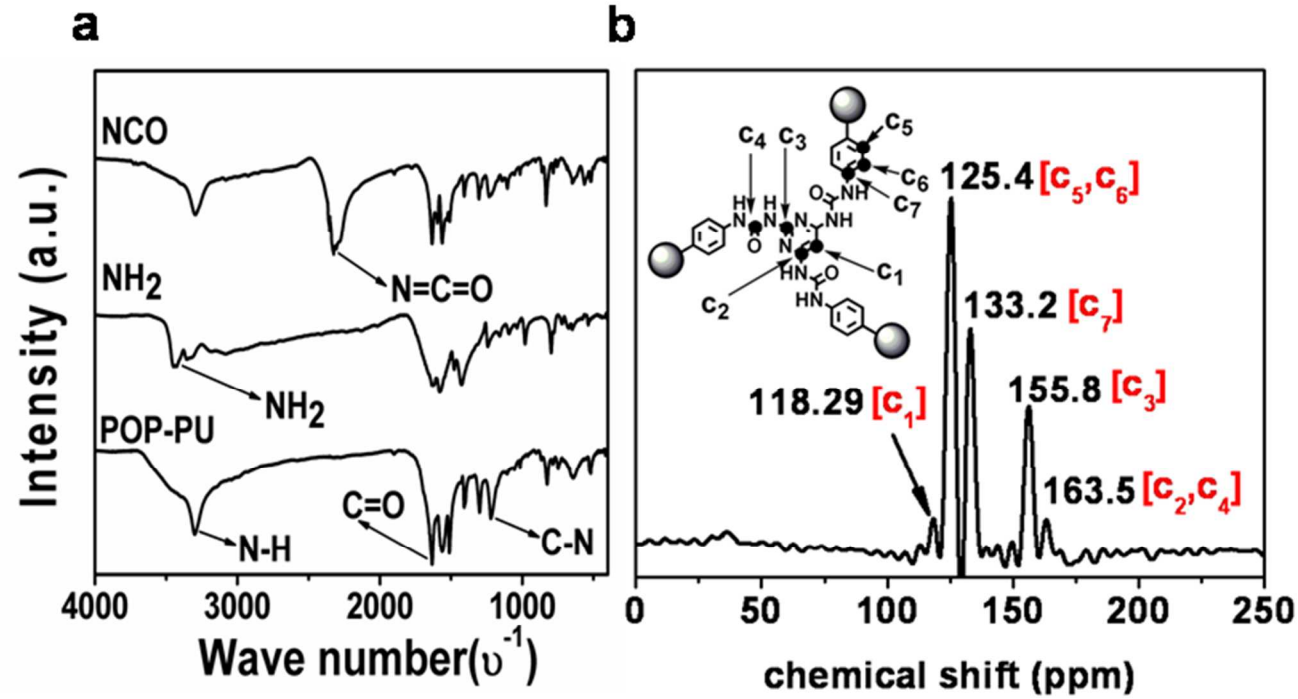
a
b
NCO
N=C=O
NH2
NH2
POP-PU
N-H
C=O
C-N
Intensity (a.u.)
4000
3000
2000
1000
Wave number(υ-1)
C4 C3
C5
C6
C7
C1
C2
125.4 [c5,c6]
133.2 [c7]
155.8 [c3]
118.29 [c1]
163.5 [c2,c4]
0
50
100
150
200
250
chemical shift (ppm)

Figure 3

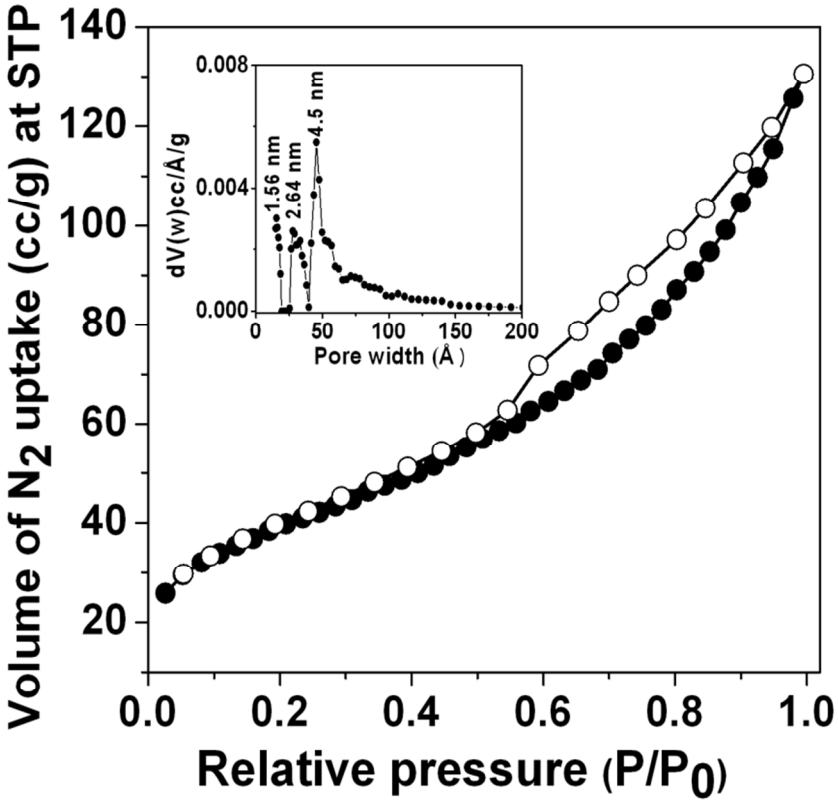
Volume of N2 uptake (cc/g) at STP
Relative pressure (P/P0)
dV(w)cc/Å/g
Pore width (Å)
1.56 nm
2.64 nm
4.5 nm

Figure 4

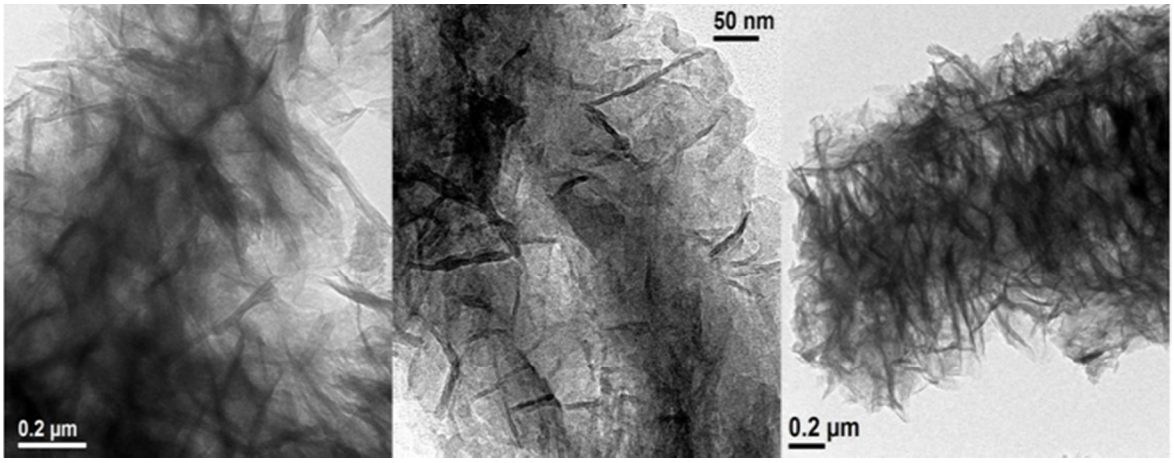

Figure 5

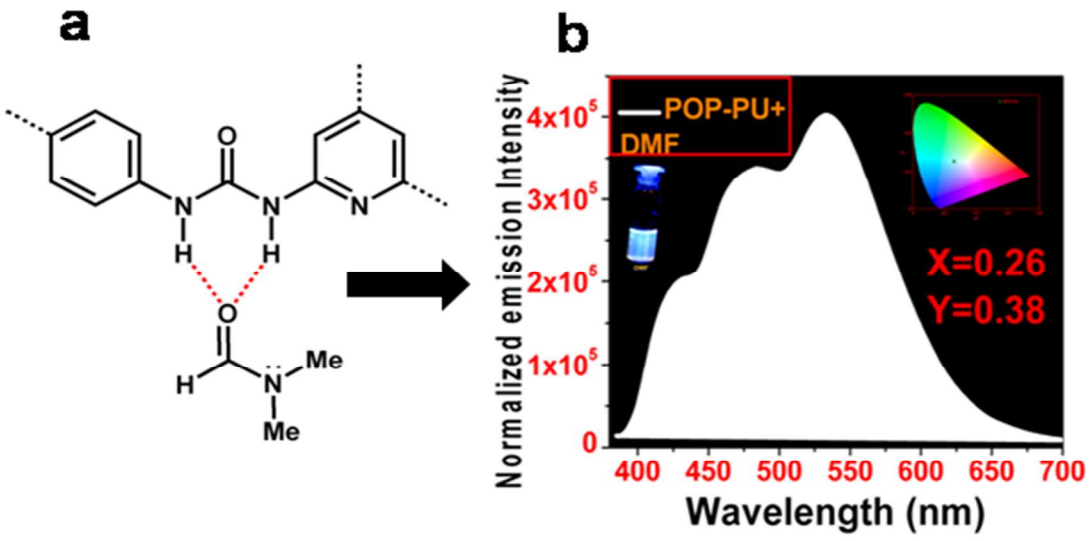
a
b
POP-PU+
DMF
X=0.26
Y=0.38
Normalized emission Intensity
4x10^5
3x10^5
2x10^5
1x10^5
0
400
450
500
550
600
650
700
Wavelength (nm)
O
N
H
Me

Figure 6

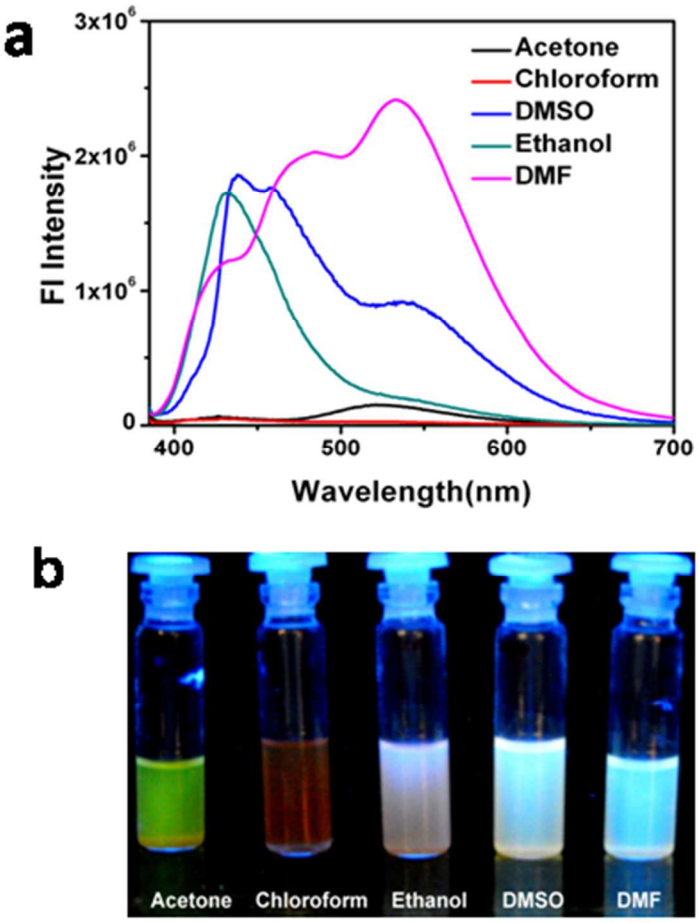
a
3x10^6
2x10^6
1x10^6
0
FI Intensity
400
500
600
700
Wavelength(nm)
Acetone
Chloroform
DMSO
Ethanol
DMF
b
Acetone
Chloroform
Ethanol
DMSO
DMF

Figure 7

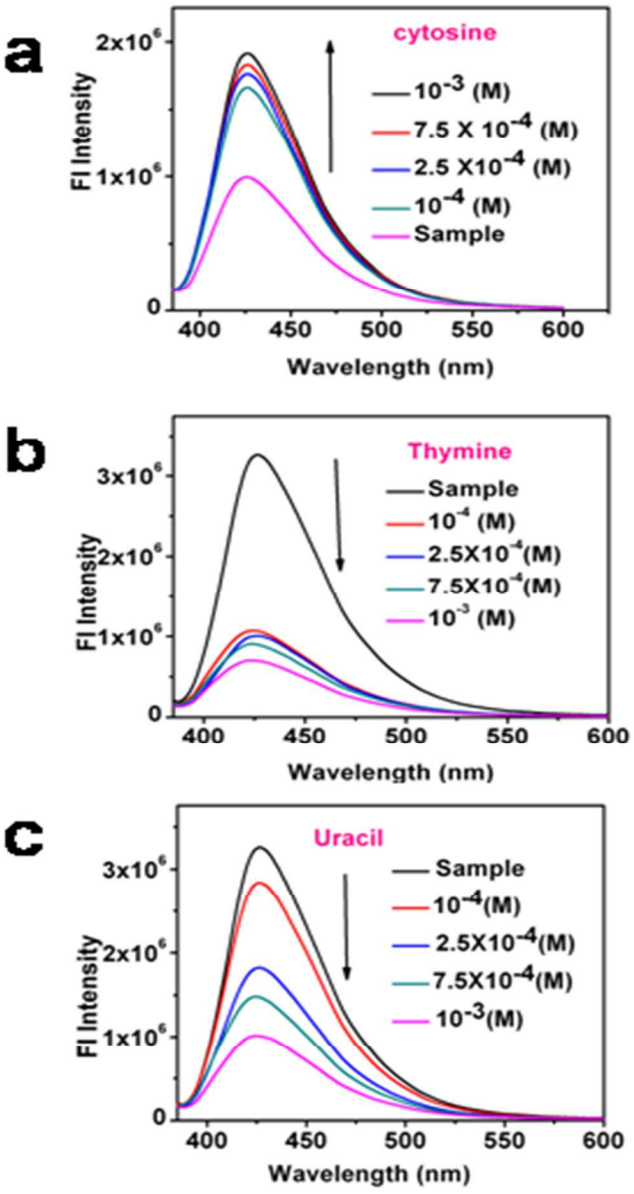
a
cytosine
FI Intensity
2x10^6
1x10^6
0
400
450
500
550
600
Wavelength (nm)
10^-3 (M)
7.5 X 10^-4 (M)
2.5 X10^-4 (M)
10^-4 (M)
Sample
b
Thymine
FI Intensity
3x10^6
2x10^6
1x10^6
0
400
450
500
550
600
Wavelength (nm)
Sample
10^-4 (M)
2.5X10^-4(M)
7.5X10^-4(M)
10^-3 (M)
c
Uracil
FI Intensity
3x10^6
2x10^6
1x10^6
0
400
450
500
550
600
Wavelength (nm)
Sample
10^-4(M)
2.5X10^-4(M)
7.5X10^-4(M)
10^-3(M)

Figure 8

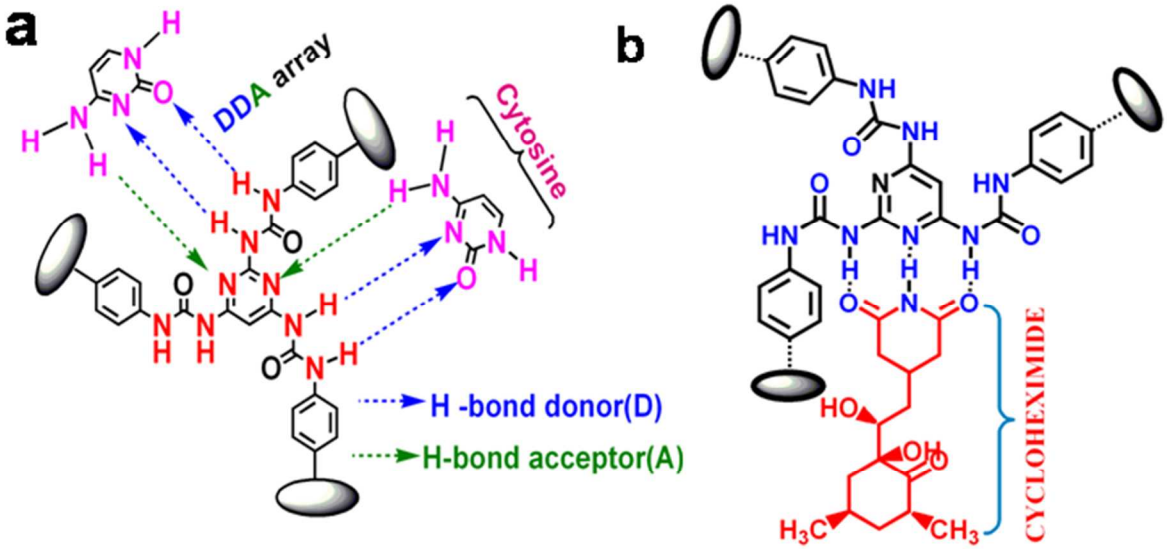
a
DDA array
Cytosine
H -bond donor(D)
H-bond acceptor(A)
b
CYCLOHEXIMIDE

Figure 9

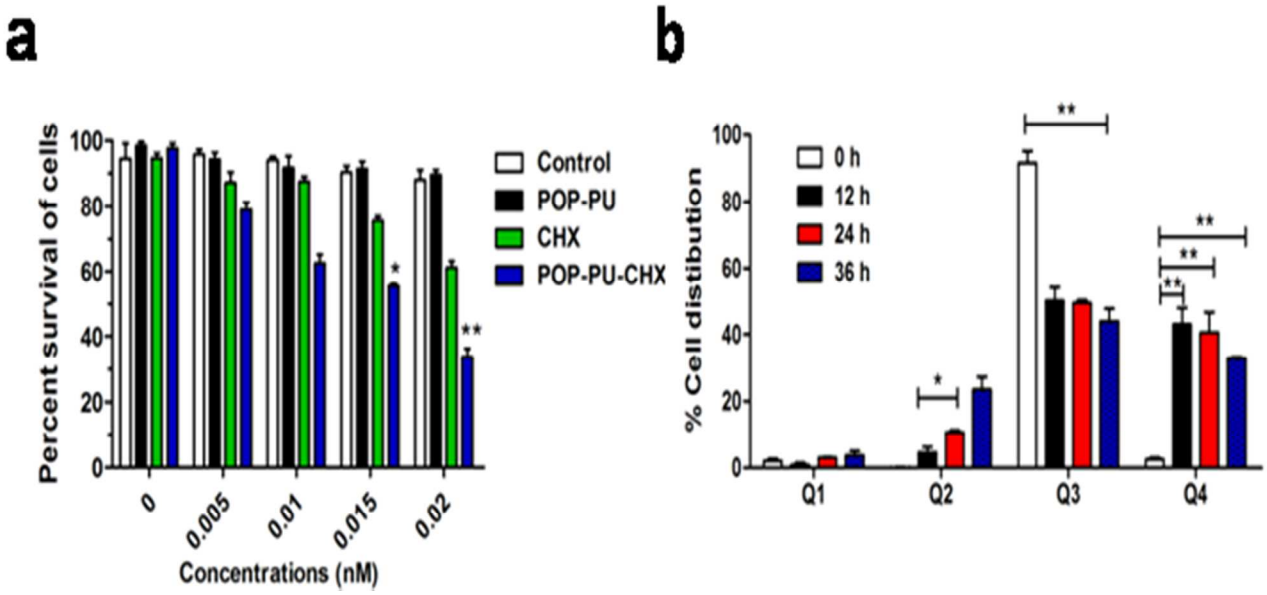
a
Percent survival of cells
100
80
60
40
20
0
Control
POP-PU
CHX
POP-PU-CHX
*
**
0
0.005
0.01
0.015
0.02
Concentrations (nM)
b
% Cell distibution
0 h
12 h
24 h
36 h
**
*
**
**
**
Q1
Q2
Q3
Q4

Figure 10

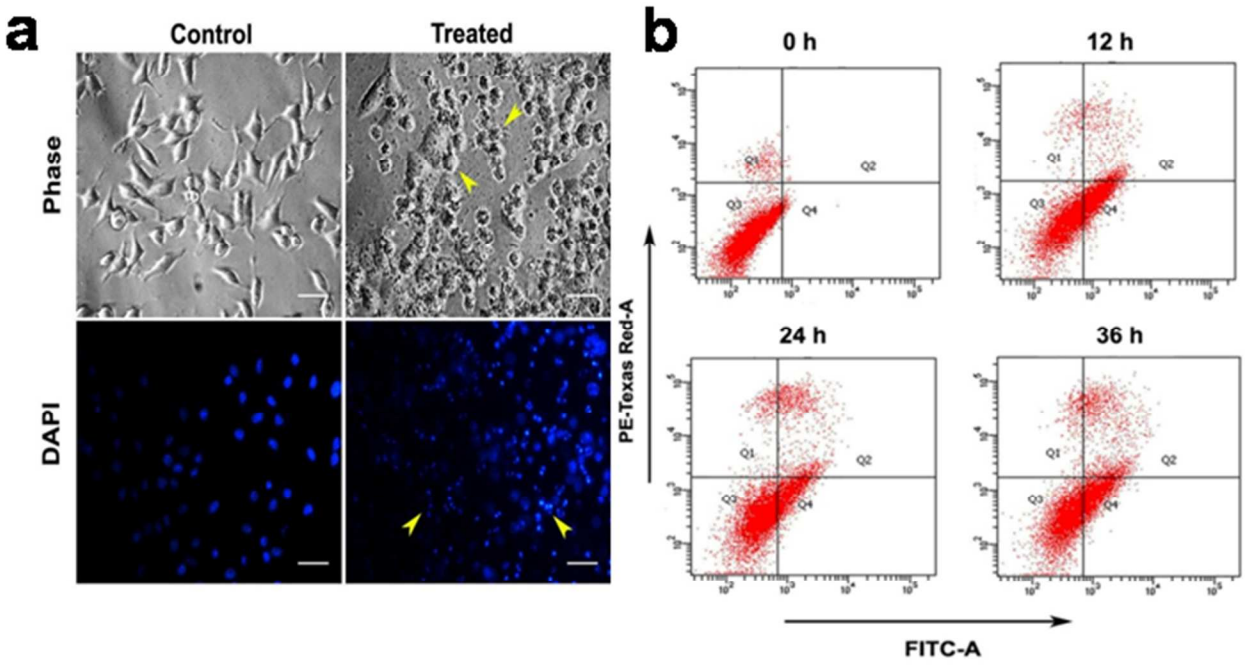
a
Control
Treated
Phase
DAPI
b
0 h
12 h
24 h
36 h
PE-Texas Red-A
FITC-A
Q1
Q2
Q3
Q4

Figure 11

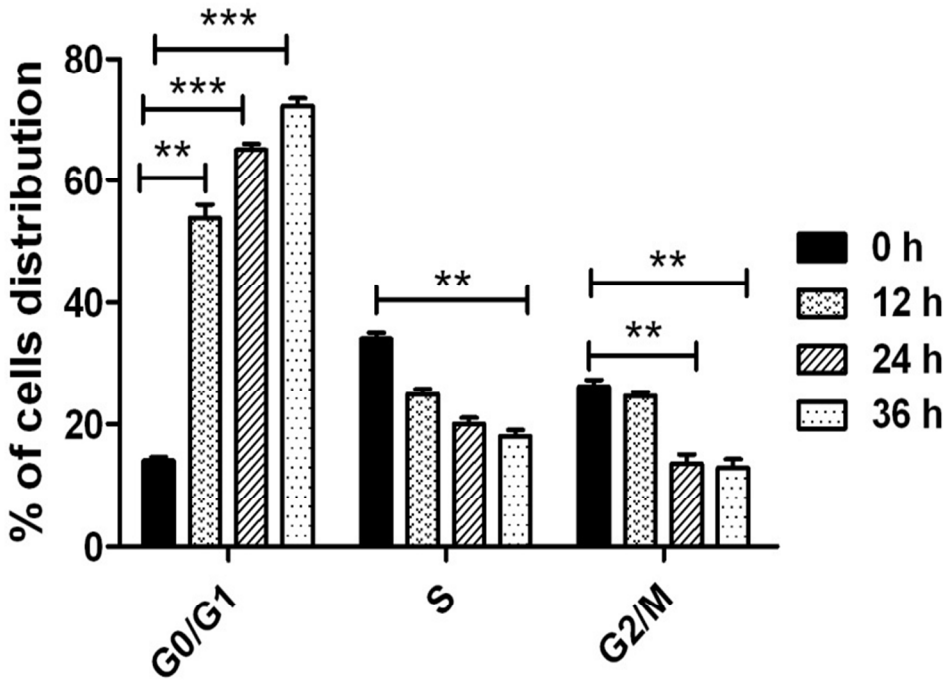

Figure 12

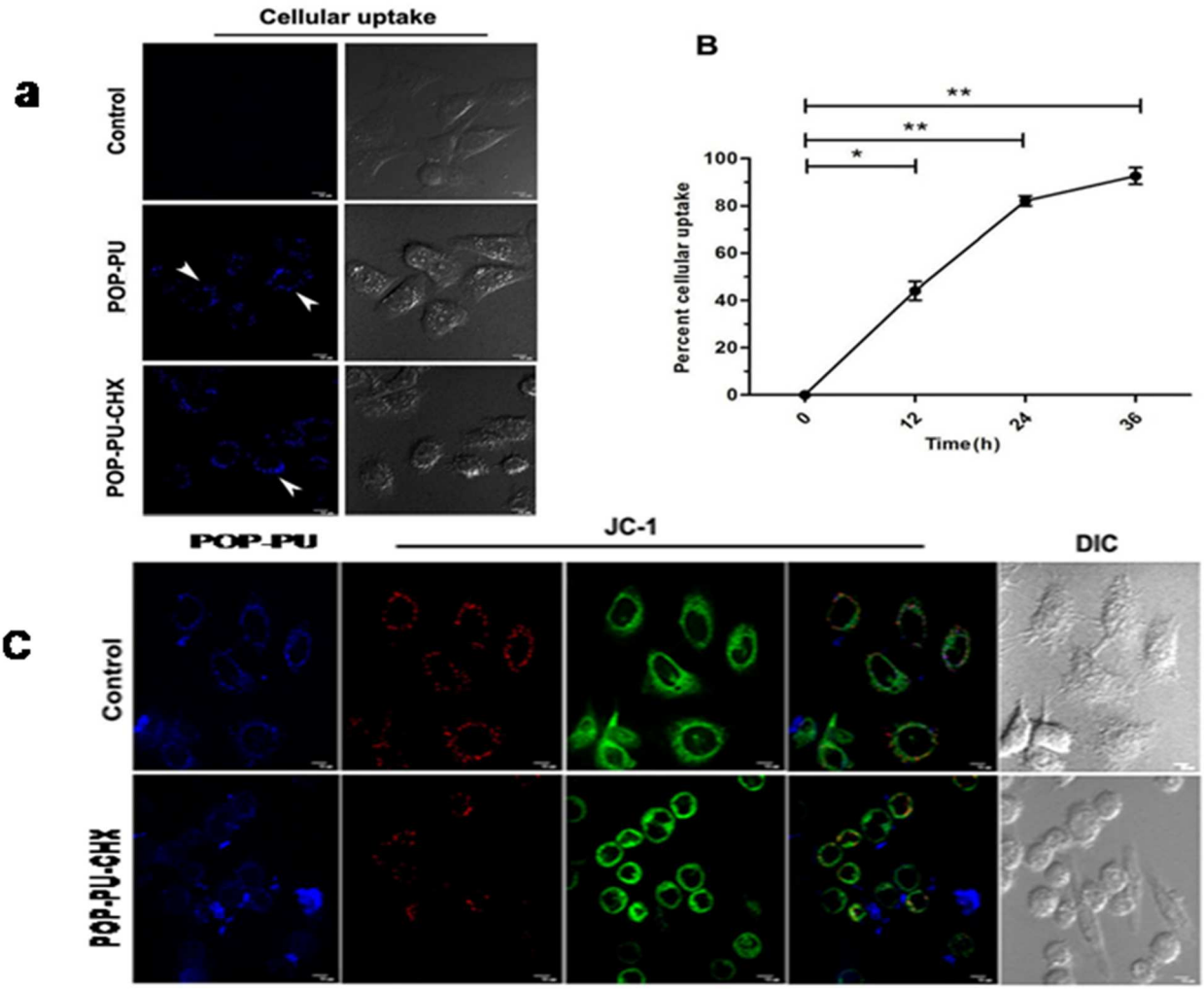
a
Cellular uptake
Control
POP-PU
POP-PU-CHX
B
Percent cellular uptake
Time (h)
0
12
24
36
100
80
60
40
20
0
**
**
*
c
POP-PU
JC-1
DIC
Control
POP-PU-CHX

Table of Contents